

Continuous Marker Patterns for Representing Contact Information in Vision-based Tactile Sensor: Principle, Algorithm, and Verification

Mingxuan Li, Lunwei Zhang, Tiemin Li, Yao Jiang, *Member, IEEE*

Abstract—Tactile sensing is an important way for robots to perceive and interact with the environment. Vision-based tactile sensors have been widely developed because of their multimodal measurement function, simple structure, and high resolution. The marker pattern method is the most popular method for vision-based tactile sensors to represent contact information. However, the current mainstream used method, distributed mark pattern (DMP), does not fully exploit the performance advantages and has limitations in terms of precision, resolution and reliability. This article innovatively proposes the idea of continuous marker pattern (CMP) and three basic design principles to improve measurement performance. A specific implementation of CMP and the corresponding information extraction algorithm are introduced in detail. We also develop a simulation process and sensor prototypes to verify the proposed method. Some comparative experiments on measurement performance were carried out to show that the tactile sensors with CMP outperformed DMP regarding measurement precision, resolution, and reliability.

Index Terms—Tactile perception, contact information, marker pattern, vision-based tactile sensor.

I. INTRODUCTION

Robots have been increasingly used in humans' daily lives, such as caregiving, health care, and education [1], which requires robots to be safer, more reliable, and intelligent. Therefore, autonomous sensing has become a core capability for robots to interact with the external environment [2], humans [3], and other robots [4].

Tactile perception is a general term for stimuli such as contact, slip, and pressure sensations. By equipping robots with multimodal tactile sensors that can sense external stimuli, robots can make autonomous decisions based on feedback and achieve contact interaction behaviors like humans [5]. In the past years, researchers have developed many different types of tactile sensors [6] and installed them on the robots [7], [8], thus giving them powerful tactile perception capability. Tactile sensors can be divided into two main forms: array-type tactile sensors and tactile image sensors.

The array-type tactile sensors measure contact distribution characteristics by integrating multiple units with independent measurement capabilities, including piezoresistive [9], piezoelectric [10], capacitive [11], and magnetic-based [12]. These

tactile sensors have a high-speed response, compact structure,

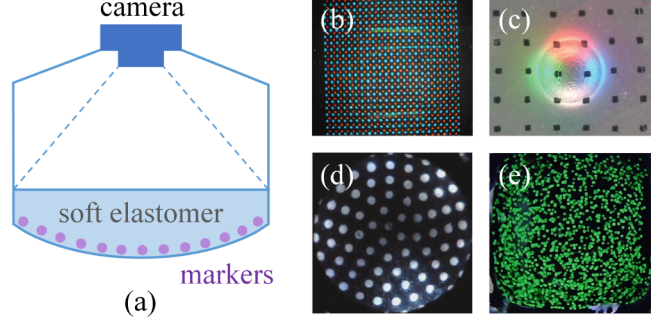


Fig. 1. (a) Components of vision-based tactile sensor. (b)-(e) Typical marker patterns: (b) GelForce [19]; (c) Gelsight [20]; (d) Tactip [21]; (e) ETH's Full-Resolution Optical Tactile Sensor [26].

and extensive range. They have been widely used as e-skin devices. However, limited by the integration process and complex hardware circuit, their measurement resolution is low. In addition, the properties of measurement units entirely determine the type of tactile information that can be perceived, so the perceptual information is relatively single, and it is challenging to meet the measurement needs of multimodal tactile information. Therefore, although the array-type tactile sensors are suitable for the sensing skin arranged on the robot arm or trunk, when it comes to the requirements of high-resolution and multimodal measurement, like robot finger, such sensors are not the best choice.

The tactile image sensors [13], also known as vision-based tactile sensors, use a soft elastomer as the contact surface, output the surface deformation information during the contact by image acquisition devices, and obtain the required contact information by reconstruction algorithms [see Fig. 1(a)]. These sensors often provide simple structure, easy preparation, and high-resolution advantages. Moreover, through the design of algorithms, multimodal tactile sensory information can be obtained (e.g., contact morphology [14], distribution force [15], slip [16], friction coefficient [17], and object hardness [18]). Several representative vision-based tactile sensors have been developed, including GelForce [19], GelSight [20], Tactip [21],

This work was supported in part by the National Natural Science Foundation of China under Grant 51705274 and a grant from the Institute for Guo Qiang, Tsinghua University.

Mingxuan Li, Lunwei Zhang, Tiemin Li and Yao Jiang are with the Institute of Manufacturing Engineering, Department of Mechanical Engineering, Tsinghua University, Beijing 100084, China (e-mail: mx-li19@mails.tsinghua.edu.cn; zlw21@mails.tsinghua.edu.cn; ltm@mails.tsinghua.edu.cn; jiangyao@mail.tsinghua.edu.cn).

FingerVision [22], and DIGIT [23]. Using vision-based tactile sensors have become a common method in robot gripping and manipulation.

From the basic configuration and operation principle of vision-based tactile sensors, obtaining contact information of the soft elastomer is the key to achieving multimodal tactile information measurement. Researchers have mainly used two methods as follows:

Photometric stereo method: This method does not require apparent texture on the elastomer. Instead, it directly uses local light changes caused by surface deformation of soft elastomer to obtain partial contact information [13], [20]. This method is outstanding for measuring contact morphology and texture [18]. However, since contact geometry is state information rather than process information, it is difficult to measure the contact distribution force and other mechanical properties only with the contact geometry information.

Marker pattern method: By printing [20], embedding [19], or 3-D printing [24], a mark pattern is prepared on the surface or inside the soft elastomer to provide texture information. When the soft elastomer is deformed under load, the feature points in the marker pattern will move accordingly and reflect the contact deformation information [13]. Compared with the photometric stereo method, although this method has lower resolution, it can directly measure dynamic contact information like distribution force and slip. Sensors that use photometric stereo methods also tend to add a marker pattern to supplement dynamic contact information (e.g., Gelsight [20]).

Fig. 1(b)-1(e) show some typical marker patterns: GelForce arranged two layers of different colored markers in a transparent elastic body [19]; GelSight printed regular rows of square dots on the inner surface of the shading layer [20]; Tactip arranged nodule markers on the inner wall of the sensor cavity [21]; researchers from ETH embedded green particles in the soft base [25]. We refer to these commonly used marker patterns, which can be abstracted as a series of distributed markers, as "distributed marker pattern", or DMP for short.

Although the DMP method can directly and conveniently measure the physical contact from the soft elastomer, they fail to utilize the two-dimensional information on the contact surface fully. It means that DMP has obvious flaws at the contact information representation level. The following text further demonstrates that three important performance metrics of contact information representation: precision, resolution, and reliability, are limited by the distributed pattern designs.

To this end, this article proposes a new type of marker pattern for vision-based tactile sensors. It is worth mentioning that our purpose is to propose a new method to represent more precise and rich contact information rather than designing a specific sensor with high performance. We mainly focus on the description of principle, algorithm, and verification. Our method can be applied to a variety of vision-based tactile sensors with marker patterns, and can improve precision, resolution, and reliability of contact information representation. The contributions of this article include:

- 1) We propose a new method for representing contact

information in vision-based tactile sensors, which is based on the continuous marker patterns (CMP). We also elaborate on the design idea, specific implementation form, and information extraction algorithm.

- 2) We conducted comparative experiments to verify our method through a simulation process and two prototypes we developed. The experimental results show that the CMP method outperforms the DMP method in terms of precision, resolution, and reliability.

The remainder of the article is organized as follows. Section II introduces the design principles and implementation scheme of CMP. Section III describes the information extraction algorithm of CMP. Section IV constructs a simulation process for the vision-based tactile sensors with a marker pattern and describes the experimental verification. Section V develops two prototypes with CMP and DMP respectively, and describes the comparative experiments. Section VI concludes this article.

II. MARKER PATTERN DESIGN: PRINCIPLES AND SOLUTION

This section focuses on analyzing the inherent performance defects of DMP and the design principles and optimal implementation of marker patterns.

A. Performance defects of DMP

For the marker pattern method, contact information representation is using features in a marker pattern to represent the deformation of soft elastomer. The core function of marker patterns is to provide meaningful characteristic information, thus facilitating the acquisition of contact information by extraction algorithm. Therefore, the more affluent, precise, and reliable the information represented from the marker patterns, the higher the precision, resolution, and reliability of the sensors.

The currently used DMP comprises a series of distributed markers, usually small prints or objects. The geometric centers of these markers are called "measured marker points", and the displacements of them are used to characterize the deformation information. Therefore, the main task of contact information extraction is to achieve the recognition and tracking of measured marker points.

Recognition of measured marker points. Algorithms such as speckle detection can extract the markers in the image [22]. The centers of the corresponding markers can determine the two-dimensional location of each measured marker point.

Tracking of measured marker points. The marker points obtained from identification processing are unorganized sets. It is necessary to match the same measured marker points in consecutive frame images to obtain the displacement. This process is also known as image registration. As for DMP, only the non-rigid point-set matching methods can be used since there is no rigid relationship among the points. An easy-to-implement method [see Fig. 2(a)] is based on the fact that each measured marker point has a small amount of position change between two adjacent frames. A matching relationship between two points can be established by searching for the nearest point

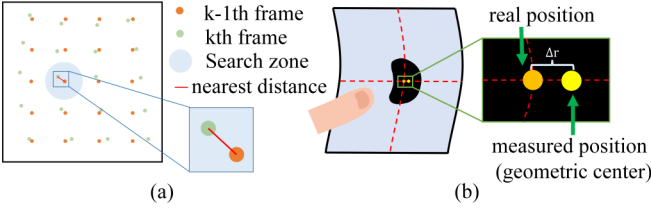


Fig. 2. (a) Marker tracking of DMP. (b) Recognition deviations in DMP.

in the previous frame around one certain point in the current frame, which can be considered the same measured marker point. In addition, there are studies on active tracking by organizing the marker points in an orderly manner [8], [24]. These algorithms usually run in $O(n^2)$.

Although DMP is easy to prepare and has efficient information representation, there are some inherent performance defects in the principles and algorithms, including:

1) Unavoidable recognition deviations of measured marker points: During the contact deformation, markers will inevitably undergo shape distortions [see Fig. 2(b)]. Since the position of a measured marker point is determined by averaging the overall of an actual marker, its calculation will inevitably be biased when the marker is distorted. Theoretically, only when the size of this marker is infinitely small can we guarantee no distortion and obtain the measured marker point with exact coordinate.

2) Limitation of tactile information resolution: Every abstracted measured marker point is the only component that can represent the contact information and exclusively reflect at the corresponding one-dimensional point of the soft elastomer. Therefore, the maximum theoretical information density can be obtained only when the markers are infinitely dense, reaching the measurement resolution limitation.

3) Failure of recognition caused by interference: The commonness requirement of enhancing the precision and resolution is making the markers infinitely small and dense. However, as the size of these points decreases, under the influence of measurement noise, the recognition is easy to have missing data element, which reduce the reliability of recognition process.

4) Failure of non-rigid registration in tracking method: When the measured marker points spacing does not differ much from the displacement, the non-rigid registration might fail to distinguish between two adjacent points. Even if these points are intentionally arranged regularly, their relative positions change unpredictably during the contact process. This defect could potentially lead to the failure of the tracking algorithm. Therefore, as the density of these points increases, the reliability of the tracking process may decrease.

B. Basic principles of marker pattern design

The defects of DMP cannot be fundamentally remedied from the aspects of the preparation process and algorithm design. Therefore, we innovatively propose three primary and vital design principles of marker patterns for tactile sensors.

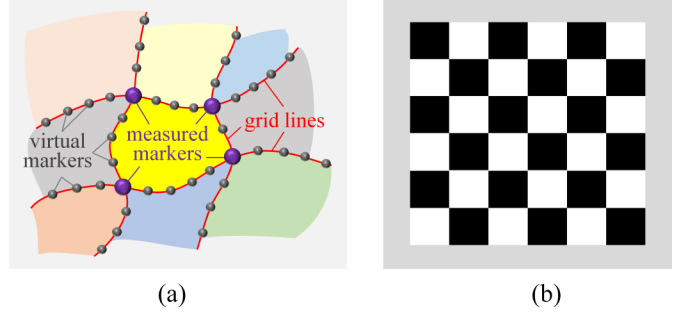


Fig. 3. (a) Essential elements in one implementation of CMP. (b) The square CMP.

1) Measured marker points are defined by interest point operator:

Instead of determining a measured marker point by the geometric center of a basic marker unit, it is uniquely determined by interest points in the marker pattern, such as the extreme value point of the local gray gradient. Theoretically, the measurement error caused by the distortions can be solved.

2) Marker patterns with two-dimensional continuity:

The components of a marker pattern that can represent contact information need to have two-dimensional continuity to make full use of the contact surface feature. Thus, the high-resolution measurement performance can be achieved without increasing the density of the basic marker units, and the issue of low recognition and tracking reliability caused by over-small and over-dense basic units can be effectively avoided.

3) A unique rigid association exists between adjacent marker points:

A physical association relationship between each marker point should exist in a marker pattern to ensure one uniquely determined rigid association between each neighboring point. The correct order of marker points can be achieved even in the case of marker points' large density and drastic changes in displacement, thus realizing rigid matching and tracking of marker points between adjacent frame images and ensuring measurement reliability.

We refer to these marker patterns, which can satisfy the above three basic design principles, as "continuous marker pattern", or CMP for short. CMP can break the restrictive relationship between the performance indicators and limitations of DMP and effectively improve the precision, resolution, and reliability in contact information representation.

C. Design scheme of continuous marker patterns (CMP)

In order to make use of CMP in practical applications, a specific and typical implementation of CMP is proposed based on the above principles. We design combinations of basic units with different colors on the surface or inside the soft elastomer, and use the gradient values of the basic pattern units to extract the ideal grid lines that intersect each other on the plane [see Fig. 3(a)]. In this type of CMP, the ideal grid lines are interwoven to form a grid with two-dimensional continuity, and the intersections of the grid lines can be uniquely defined and identified as measured marker points. In addition, multiple virtual marker points can be extracted from the grid lines, and all marker points are connected with grid lines, which builds a deterministic physical correlation between adjacent marker

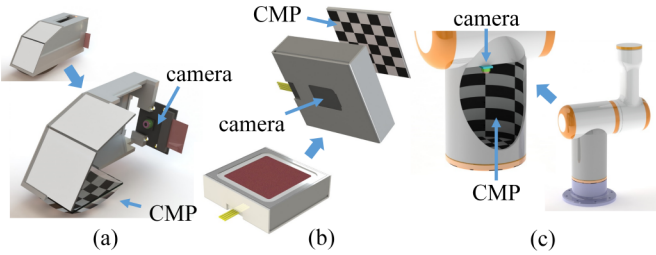


Fig. 4. Several possible application scenarios using CMP in tactile sensors. (a) Sensor for robot finger. (b) Sensor for robot skin. (c) Sensor for robot link.

points. Therefore, this design fully satisfies the design principle of CMP. Three essential elements can be abstracted from this design:

1) Ideal grid lines: Ideal grid lines without geometric dimensions are extracted from the color gradient values of the basic pattern units in a marker pattern, so their theoretical position will not be affected by the distortions of the markers. These lines are the critical elements for defining measured marker points, virtual marker points, and constructing physical association relationships of sign points.

2) Measured marker points: These points are uniquely determined by the intersection relationship of ideal grid lines that are essentially the feature points of the marker pattern.

3) Virtual marker points: The contact information carried by ideal grid lines cannot be obtained directly and needs to be discrete, so multiple discrete points are selected on the grid lines and defined as virtual marker points. They can be used as supplementary information to enhance the information density of the marker pattern.

In order to facilitate the preparation of marker patterns and simplify the complexity of algorithm designs, it is necessary to select a simple color combination for these basic pattern units. For this purpose, the blocks of alternating black and white are selected. Without loss of generality, this article uses the square CMP [see Fig. 3(b)] as the selected type of CMP for subsequent algorithm design, simulation verification, and prototype development.

D. CMP for different vision-based tactile sensors

The proposed CMP principle does not depend on a specific form of the marker pattern nor the structure and design of vision-based tactile sensors. According to the three basic principles, different styles of CMP can be designed for any sensor based on the marker pattern method. Fig. 4. illustrates several vision-based tactile sensors with CMP (the square CMP as a demonstration). For sensors based on hybrid methods (combination of photometric stereo method and marker pattern method), such as Gelsight [20], CMP can also replace the used discrete markers.

III. INFORMATION EXTRACTION ALGORITHM OF CMP

For vision-based tactile sensors with CMP, the deformation information of the soft elastomer is represented by ideal grid lines in the marker pattern and calculated by the displacement

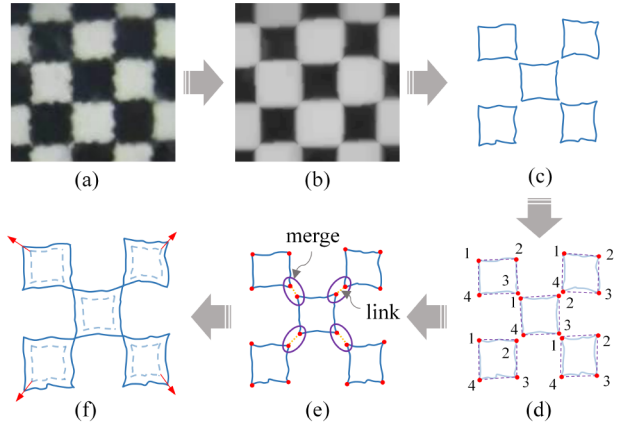


Fig. 5. Contours stitching method. (a) Original image. (b) Image pretreatment. (c) Contour extraction. (d) Polygon fitting. (e) Corner merging. (f) Construction of ideal grid lines.

of measured and virtual marker points. Therefore, the core task of the information extraction algorithm is to detect ideal grid lines and establish and track marker points. This section takes the selected square CMP to introduce the extraction algorithm, but the corresponding design idea and process can be extended and applied to the general form of CMP, not limited to the structure of sensors.

A. Detection of ideal grid lines

As for the square CMP, the ideal grid lines are a set of edges connected at the corners. Limited by the preparation process, it is difficult to guarantee the absolute clarity of the checkerboard edges and connections, resulting in a large number of noise and vacancies in the grid lines obtained using an edge detection algorithm. We propose the contour stitching method to get the ideal grid lines, shown in Fig. 5. The complete procedure of the algorithm is given below:

Image pretreatment. Convert the input image into a greyscale image, remove illumination influence, and denoise the image. Repair the small missing color blocks by using open and closed operations in a loop and separate the checkers from each other by erosion operations [see Fig. 5(b)].

Contour extraction. Extract all contours in the image, and remove uninteresting contours based on area, perimeter, and position [see Fig. 5(c)]. This step removes the interference generated by the background color and noise, keeping only the outlines of checkers.

Polygon fitting. For the square CMP, each basic unit (checker) has four corners. Use polynomial fitting on all contours to obtain the four corners of each checker. According to the orientation relative to the checker center, we number the four corners of each checker into corner 1, 2, 3, and 4 [see Fig. 5(d)], which represents their position in each checker. Thus, the topological connection relationship of corners within each checker is obtained.

Corner merging. Traverse all the corners and merge the neighboring ones to construct a connection between the contours of neighboring checkers [see Fig. 5(e)]. Conditions for determining whether to merge corners include the distance between the checkers, the distance between the corners, and

Algorithm 1: MERGECORNERS($\Phi, n, L_{checker}, L_{corner}$):

Input: The set of checkers Φ , number of checkers n , threshold distance for checkers $L_{checker}$, threshold distance for corners L_{corner} .

Output: The set of checkers after corner merging Φ .

Begin

```

1: for  $i \leftarrow 1$  to  $n$  do
2:   for  $j \leftarrow 1$  to  $n$  do
3:     Initialize:  $l_{ij} \leftarrow$  The distance between the centers of  $\Phi_i$  and  $\Phi_j$ 
4:     if  $l_{ij} < L_{checker}$  then /* Narrow the search area */
5:       Initialize:  $k_1, k_2$ 
6:       for  $k_1 \leftarrow 1$  to  $4$  do /* Select corner  $k_1$  from checker  $\Phi_i$  */
7:          $k_2 \leftarrow \text{SELECTK2}(k_1)$  /* Select corner  $k_2$  from checker  $\Phi_i$  */
8:         Initialize:  $l_{k12} \leftarrow$  The distance between corner  $k_1$  and  $k_2$ 
9:         if  $l_{k12} < L_{corner}$  then /* Merge corners must be adjacent */
10:          Merge corner  $k_1$  in  $\Phi_i$  and corner  $k_2$  in  $\Phi_j$ 
11:        end if
12:      end for
13:    end if
14:  end for
15: end for
16: return Merged set  $\Phi$ 
function SELECTK2( $k_1$ ) /* Select corners based on relative position */
1: if  $k_1 = 1$  return 3
2: else if  $k_1 = 2$  return 4
3: else if  $k_1 = 3$  return 1
4: else if  $k_1 = 4$  return 2
5: end if
end function
End

```

each corner's serial number. The details of the algorithm that runs in $O(n^2)$ are shown in Algorithm 1. $L_{checker}$ and L_{corner} are set according to the actual situation. Thus, the topological connection relationship within the whole checkerboard is obtained.

Construction of ideal grid lines. Perform an expansion operation on the outline to repair the shrinkage deviation. Connect all the contours and remove the redundant lines to build the ideal grid lines [see Fig. 5(f)].

B. Establishment and tracking of measured marker points

With the grid lines obtained previously, measured marker points can be established by determining the intersections of the lines, namely the checkerboard corners. To entirely use the association relationship constructed by the ideal grid lines, we propose the gridline pointer method to achieve rigid and reliable tracking of measured marker points, as shown in Fig. 6. The complete procedure of the algorithm is given below:

Pointer establishment. Previously we have obtained the connectivity of the entire checkerboard grid, which is equivalent to the topological connectivity graph. We can set four pointers for each point to its neighbors using the gridline connection [see Fig. 6, take corner a_1 and c_1 as examples].

Point organization. Based on the topological connectivity graph, we can use pointers to get the path between any two points. For example, the path from a_1 to b_1 in Fig. 6 is {right (to a_2), down (to c_1), right (to c_2), up}. The most upper-left point is selected as the starting point. From that point, we

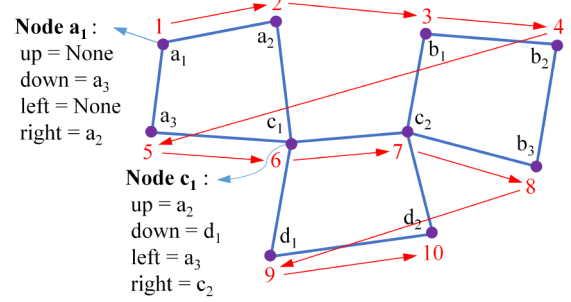


Fig. 6. Gridline pointer method. Through the pointer of each point to its neighbor, we can easily traverse and number each point in the order of red arrows.

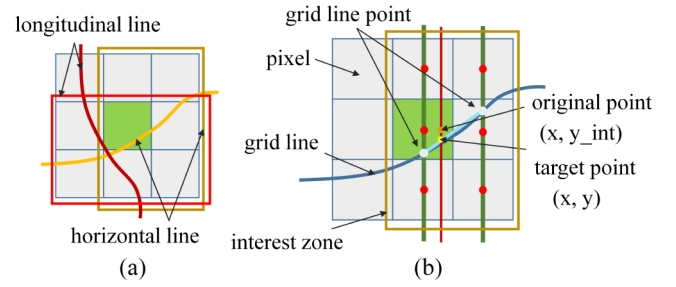


Fig. 7. Local sub-pixel correction method. (a) Select the yellow zone for the horizontal line and the red zone for the longitudinal line. (b) Use binomial fitting and linear approximation to obtain the target point.

traverse each point in the connected graph and number them. Thus, an organized set of points can be obtained.

Point tracking. In different frame images, points with the same number are the same point since they have the identical position in the original marker pattern. Such a point-set registration is rigid. By matching the set of points according to their numbers, the tracking of the marker points can be achieved.

C. Establishment and tracking of virtual marker points

Virtual marker points are established to enrich the contact information representation. They can be obtained by discretization of ideal grid lines. However, the previously obtained grid lines are formed by pixel dots on the outlines of checkers and thus have pixel-level widths that do not meet the requirements of wireless widths. It means that direct extraction only yields points with pixel-level accuracy. We propose the local sub-pixel correction method to obtain the virtual marker points, shown in Fig. 7. A complete procedure of the algorithm is given below:

Discretization of grid lines. Choose two adjacent measured marker points and select a certain number of virtual marker points, as the original point, on the gridline between them. The benchmark for discretization is to have these points equally spaced in the x or y direction. Perform the operation for all measured points.

Local zone selection. Grid lines can be divided into horizontal and longitudinal lines according to their shape before deformation. For virtual marker points on different grid lines,

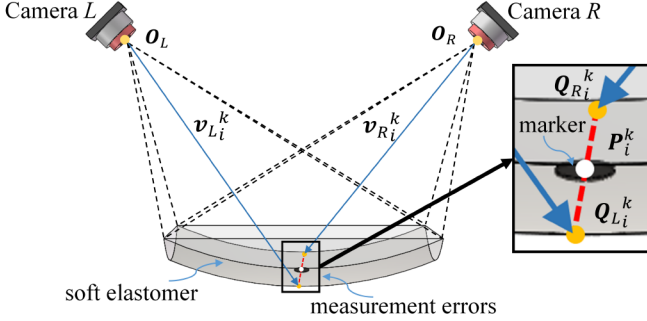


Fig. 8. Binocular stereo vision for 3-D position measurement. In the non-ideal case, the extension lines of the two direction vectors do not have intersection points. A correction method based on the common normal is used to determine the 3-D coordinates of the markers.

selecting different local zones allows only valid information to be retained, making computing more efficient [see Fig. 7(a)].

Quadratic fitting. Each local zone contains six pixels. Calculate the gray gradient of pixels in the local zone of each virtual marker point. For every three neighboring pixels, a local maximum gradient position corresponding to a grid line point can be found by the quadratic fitting method. Two grid-line points with extreme gray-level gradient can be found in each local area [see Fig. 7(b)].

Sub-pixel correction. Since we previously discretized with equal spacing in the x or y direction, the coordinates of a virtual marker point in that direction are determined. Based on the known coordinates of the two grid-line points, the linear approximation can obtain the target point and determine the coordinates in another direction.

Since each set of virtual marker points is determined by the gridline between two adjacent measured marker points, the point-set tracking can be achieved using the already numbered measured marker points.

In the following sections, we will verify the proposed principle and algorithm through the comparative experiments in the simulation environment and the actual environment.

D. The potential of machine learning approaches in CMP

Machine learning techniques have been successfully applied to computer vision and have accomplished many challenging tasks. In the field of vision-based tactile sensing, researchers have been exploring and advancing the application of machine learning methods [14], [18], [25].

The information extraction of CMP is a process of detecting features in the pattern, and the specific algorithm depends on the actual needs of tactile sensors. Although the traditional computer vision approach is chosen for simplicity and generality in this article, we believe that the use of learning methods in CMP information extraction is very promising. Since tactile information extraction and camera calibration of CMP are similar to a certain extent, using a convolutional neural network (CNN) to improve the accuracy and robustness of the detection algorithm has high reference [32]. This inspires us to explore the potential of using learning methods for representing tactile information in the follow-up work.

IV. SIMULATION EXPERIMENTS

In practical applications, other objective factors (e.g., material selection, preparation process, and experimental conditions) can also impact the representation of contact information. Therefore, even if the CMP method is feasible in principle, those factors can still lead to failure. To this end, this section builds a simulation process for vision-based tactile sensors using the marker patterns method. Under the condition that other objective factors are excluded, we verify the proposed principle's rationality and the effectiveness of algorithmic process in the simulation.

A. 3-D position measurement of marker points

Using the algorithm of CMP proposed, we can only obtain the marker points' two-dimensional position and displacement. In order to verify whether the extraction of contact information is reliable and effective, we need to compare the reconstructed contact information with the actual value. Thus, it is necessary to expand the 2-D information to 3-D, i.e., to measure the 3-D positions of marker points. A method based on binocular stereo vision is given, as shown in Fig. 8.

Cameras L and R have known internal and external parameters. Let \mathbf{Q}_{Li}^k and \mathbf{Q}_{Ri}^k denote the position of marker point i in the view field of camera L and camera R . According to \mathbf{Q}_{Li}^k and \mathbf{Q}_{Ri}^k , the line direction from the camera to the marker point can be determined. Let \mathbf{v}_{Li}^k denotes the direction vector related to camera L , and \mathbf{v}_{Ri}^k for camera R . Due to measurement errors, the extension lines of direction vector \mathbf{v}_{Li}^k and \mathbf{v}_{Ri}^k usually do not intersect. Therefore, a correction method based on the common normal is used. The common normal vector of the vector \mathbf{v}_{Li}^k and \mathbf{v}_{Ri}^k can be calculated as

$$\mathbf{Q}_{Li}^k \mathbf{Q}_{Ri}^k = \mathbf{O}_R \mathbf{O}_L + t_L \mathbf{v}_{Li}^k - t_R \mathbf{v}_{Ri}^k \quad (1)$$

where t_L and t_R are scaling factors. According to the orthogonality relation, they can be determined as

$$\begin{cases} \mathbf{v}_{Li}^k \cdot \mathbf{Q}_{Li}^k \mathbf{Q}_{Ri}^k = 0 \\ \mathbf{v}_{Ri}^k \cdot \mathbf{Q}_{Li}^k \mathbf{Q}_{Ri}^k = 0 \end{cases} \quad (2)$$

Hence, the 3-D position of the marker point i in the spatial coordinate system is

$$\mathbf{P}_i^k = \frac{(\mathbf{Q}_{Li}^k + t_L \mathbf{v}_{Li}^k) + (\mathbf{Q}_{Ri}^k + t_R \mathbf{v}_{Ri}^k)}{2} \quad (3)$$

Since \mathbf{v}_{Li}^k is not parallel to \mathbf{v}_{Ri}^k , the common normal $\mathbf{Q}_{Li}^k \mathbf{Q}_{Ri}^k$ must exist, so we can always use this method to calculate the 3-D positions. The contact morphology and deformation field of soft elastomer surface can be obtained by interpolating these 3-D coordinates.

B. Simulation process for marker patterns

Vision-based tactile sensors have been proven to be difficult to simulate because multiple factors and conditions need to be considered to get close to realistic perceptual outputs [26]. At present, the existing simulation methods are usually based on PyBullet [26], Gazebo [27], Unity [28], physics-based rendering (PBR) [29], and finite elements models (FEM) [30], which can meet the simulation requirements of specific

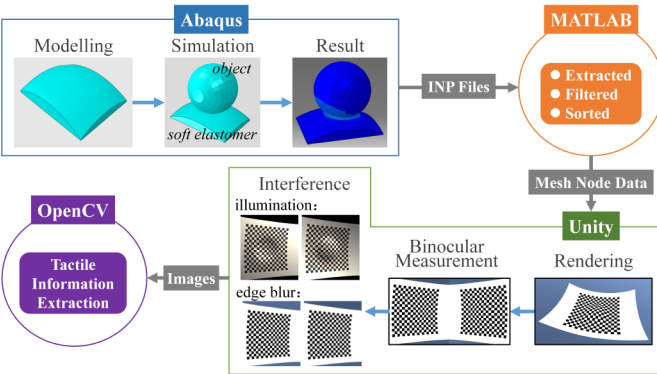


Fig. 9. Simulation process of vision-based tactile sensor. The contact characteristics are simulated using Abaqus, the marker pattern is rendered by Unity, and the proposed algorithms are used to achieve tactile information extraction.

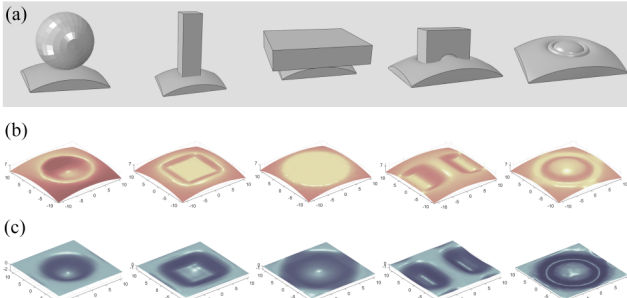


Fig. 10. Contacting with different objects. (a) Contact of five objects with soft elastomer. (b) 3-D contact morphology reconstruction. (c) 3-D contact displacement field reconstruction.

practical characteristics but is challenging to simulate the mechanical and optical properties of sensors completely. This article uses a variety of engine combinations, including Abaqus, Unity, MATLAB, and OpenCV [see Fig. 9], to build a simulation process especially suitable for vision-based tactile sensors with marker patterns.

1) Contact characteristic simulation: We use Abaqus to simulate and analyze the contact dynamics. First, the soft elastomer and the object model are constructed in Abaqus, and the material and mechanical properties are set similarly to the practical values of a silicone elastomer. Then, the model mesh is divided, and the contact force is applied to simulate the physical process when the soft elastomer is in contact with an object. Finally, the point cloud data of the soft elastomer is derived from the simulation results. They can be extracted, filtered, and sorted by MATLAB to obtain the 3-D position and contact information of all mesh nodes of the elastomer surface.

2) Marker patterns rendering: The marker pattern needs to be rendered along with the model. We choose Unity since this engine has powerful graphics rendering capabilities. Based on the point cloud data of the soft elastomer, the soft elastomer model is constructed in Unity using triangular facets. The corresponding triangular facets are colored and rendered to build the marker pattern, and the contact information of

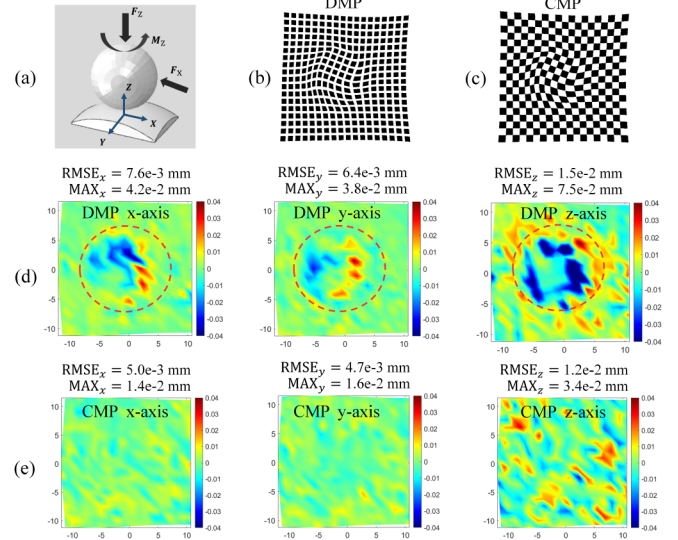


Fig. 11. Comparison of the displacement field reconstruction precision. (a) Simulation of contact between the sphere and the soft elastomer. (b), (c) Deformation of DMP and CMP. (d), (e) Error distribution of displacement corresponding to the two patterns. The red circle shows the contact area with significant local errors.

elastomer surface is reflected by the edge line displacement of these facets. Finally, the internal and external parameters of an added camera are adjusted according to the actual value to capture the marker pattern precisely. Different degrees of information interference, such as uneven illumination and edge blurring of the marker pattern, can be flexibly introduced to more realistically simulate the characteristics of the actual vision-based tactile sensor.

3) Tactile information extraction: For the images outputted from Unity, use OpenCV to realize the information extraction of marker patterns according to the relevant algorithm. The result can be compared with the set-theoretical value to realize the closed-loop simulation verification.

This simulation process constructed above can be modified to apply to different vision-based tactile sensors with marker patterns, which are not limited to the CMP proposed in this article. Under the condition that other objective factors are excluded, we verify the effectiveness of the principles and algorithms. By comparing the tactile sensors with DMP, the advantages of using CMP are quantitatively reflected. The measured marker points of DMP and CMP are set as 18×18 (for CMP, measured marker points are equal to the shared inner intersections of the checks) to ensure that the number of feature points obtained is the same.

C. Verification of principles and algorithms

In this experiment, we used soft elastomer with CMP. Five typical objects with different shapes were selected. We contacted them with the soft elastomer under positive pressure in the simulation, shown in Fig. 10(a). Finite element analysis can provide us with the morphology and deformation fields during the contact. We regard them as the reference values. If

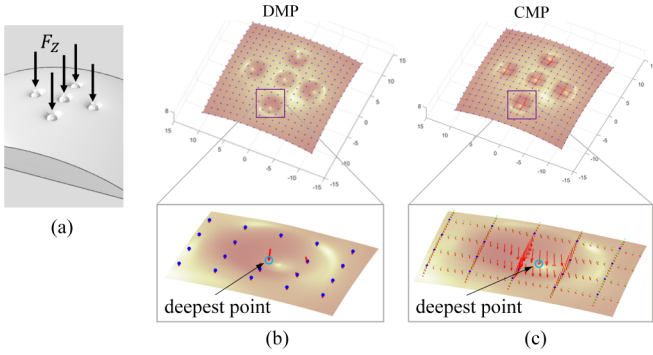


Fig. 12. Comparison of the contact morphology and displacement field reconstruction resolution. (a) Simulation of contact between the small spheres and the soft elastomer. (b), (c) Reconstruction of contact morphology and displacement field. The red lines represent the displacement, and the blue dots represent the measured mark points.

the contact morphology and deformation fields reconstructed by our method match the reference values, it proves that the CMP method is correct and effective.

The proposed information extraction algorithm was used to reconstruct the contact morphology and displacement field [see Fig. 10(b), 10(c)]. Compared with the reference values, the mean absolute errors of 3-D coordinates of all the marker points were solved. Results show that the mean absolute errors of different objects are all less than 0.02mm. Therefore, the principles and algorithms of the CMP method are verified to be feasible and effective.

D. Comparison of measurement precision

Next, the performances of the CMP method and DMP method were quantitatively compared. First, we compared the precision of them in representing the contact information. A sphere of 15 mm radius was selected to contact the soft elastomer, and the load conditions were set as follows: positive pressure $F_N = 50$ N, tangential force $F_T = 12$ N, and torque $M_Z = 50$ N·mm [see Fig. 11(a)].

Fig. 11(b), 11(c) show the deformation represented by CMP and DMP in this case. By calculating the difference between the measured and actual displacement values, and the overall error distribution of these marker points in x , y and z directions were obtained [see Fig. 11(d), 11(e)]. The results show that the root mean square errors and the maximum errors of the displacement field reconstructed based on DMP are noticeably larger than the errors of CMP, in all three directions. In addition, the error distribution of CMP is more uniform, while the reconstruction displacement field of DMP shows a significant concentration error in the contact region. In this region, the sphere was in direct contact with the soft elastomer, and the distortion was highly remarkable, so the resulting measurement error was significant. The above comparison experiment shows that the CMP method can effectively eliminate the measurement error caused by pattern distortion and show good adaptability to changes in loading conditions, which can effectively improve the precision of contact information representation.

E. Comparison of measurement resolution

Next, we compared the resolution of these two methods in reflecting the tactile information [see Fig. 12(a)]. Five small spheres of 1mm radius were selected to contact the soft elastomer, and the load condition was set to apply positive pressure of 50 N. The 3-D morphologies and displacement fields were reconstructed by the two patterns, respectively [see Fig. 12(b), 12(c)]. The reconstruction of the DMP method can only sporadically reflect the displacement at a few discrete points, which is not sufficient to reconstruct the contact morphology finely. The reconstruction of the CMP method is supplemented by introducing virtual marker points that are continuously and densely arranged along the gridlines. Therefore, the contact deformation of the elastomer surface can be presented clearly.

Observation of the pressed areas of the different spheres reveals that, as for DMP, the concentrated load has a more obvious displacement response while it was acting near a certain measured marker point; as for CMP, the reflection of the concentrated load is visible while it was acting near the measured marker points and the virtual marker points, and even if the load didn't act near these points, the virtual marker points on the surrounding gridlines could provide rich information of the displacement trend. Therefore, by establishing the virtual marker points, the CMP method can increase the information density of representation and improve loads' response-ability, thus effectively improving the resolution of contact information representation.

F. Evaluation of measurement reliability

The main factors that affect the reliability of the CMP method are illumination conditions, environmental noise, and the sensor preparation process. We adjusted the lighting conditions and pepper-salt noise within a reasonable range to test the robustness of the CMP method under different disturbances.

We use the ratio of the values of the dominant peak (in the image histogram) to the minimum peak to describe the degree of illumination interference. Results show that the algorithm works properly for ratios > 0.4 , and the algorithm did not fail at the visibility that the simulation was able to provide.

We describe the degree of noise interference in terms of signal-to-noise ratio (SNR). Results show that when $\text{SNR} < 0.95$, the algorithm starts to fail. It indicates that the CMP method is sensitive to environmental noise.

However, the interior of a tactile sensor is a structured environment. Generally, a sensor housing is opaque, and the internal optical system is fixed. As long as a sensor is not damaged during operation, the algorithm will be working in a defined environment. From this perspective, light and noise interference have limited impacts on the reliability of the CMP method in practice.

Therefore, to verify the reliability of tactile sensors based on the CMP method, research should mainly focus on the effectiveness of the rigid image registration method in a practical environment. We will present the specific

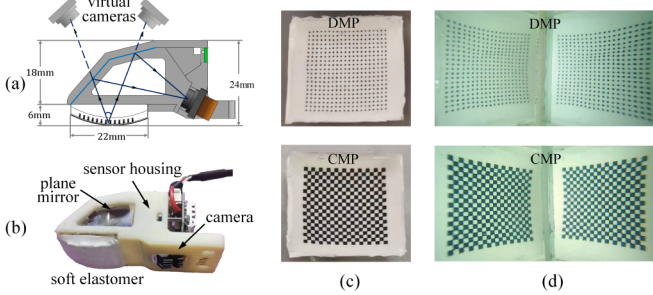


Fig. 13. Experimental prototypes of vision-based tactile sensor. (a) Optical structure based on the virtual binocular vision principle. (b) Composition of tactile sensor prototype. (c) Soft elastomers with DMP and CMP. (d) Images captured by the sensor camera.

demonstration of comparative experiments in the following section.

V. PROTOTYPE EXPERIMENTS

This section develops two sensor prototypes with CMP and DMP, respectively. It is worth mentioning that our prototypes are only used for experiments. We focus on verifying the CMP method, not designing a vision-based tactile sensor that is superior to other similar devices like GelForce [19] and GelSight [20]. Instead, our prototype can provide a reference for other tactile sensors to apply the proposed CMP. Based on the above concept, we pay more attention to the relative performance of CMP and DMP method than the performance of the sensor itself. The precision, resolution, and reliability we mentioned also indicate only relative advantages between the CMP method and DMP method.

Several comparative experiments were carried out. It seems redundant to repeat the comparison already performed in the simulation. However, we stress that the two sections conduct experiments with different emphases. In the simulation, the reference value of the contact information is available and the disturbances can be controlled, so we focus on validating the method under ideal conditions. Through prototype experiments, we are more interested in comparing the performance of the two methods in practical application.

A. Experimental prototypes

We designed our prototypes based on the structure of Tac3D [31]. The virtual binocular vision principle is adopted for 3-D measurement. As shown in Fig. 13(a), two plane mirrors are added to construct the optical path structure. Only one camera is needed to achieve the same measurement effect as the binocular camera, which provides the advantages of compact structure and simple hardware.

The construct of our tactile sensor prototypes developed is shown in Fig. 13(b), including soft elastomer, plane mirror elements, camera, and sensor housing. A custom micro camera was used with a lens having a field of view of 100°, a focal length of 2.6 mm, an aperture number of 1.3, and an image resolution of 1024 x 768 pixels. Lighting was provided by the built-in LED light source.

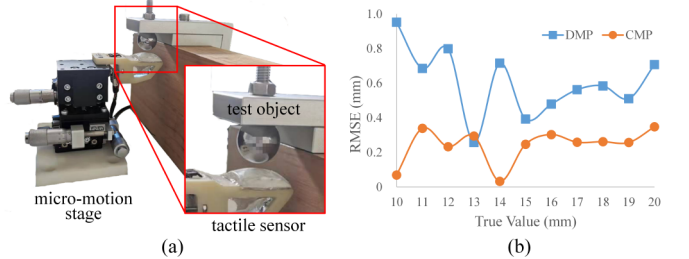


Fig. 14. Precision comparison of tactile sensors. (a) Experimental platform (b) Comparison of sphere diameter fitting results.

The soft elastomer of the tactile sensor consisted of a transparent body, a marker pattern, and a surface shading layer. The overall size was 22 mm × 22 mm × 6 mm, and the contact surface was designed as a sphere with a radius of 27 mm to ensure good contact. The transparent body was made of PDMS, and the surface shading layer was made of K704L silicone. The marker pattern was printed on the inner surface of the shading layer. We prepared two soft elastomers with DMP and CMP, respectively [see Fig. 13(c)]. DMP included 20×20 markers, and CMP contained 20×20 inner corners (common intersections of the checks). The images taken at the two virtual camera positions fell exactly on the left and right half-planes of the real camera field of view, as shown in Fig. 13(d).

Experiments were run on a desktop PC: i7-9750H processor at 2.59 GHz and 16.0 GB of RAM. The processing frequencies for the two methods are 24 Hz (DMP) and 18 Hz (CMP), with C++ code. The main factor that affects the speed of sensors is the camera frame rate, so there is no significant difference in speed performance between the two methods in real-world use. The computation complexity of the CMP method is also tested. The corresponding algorithm can be carried out online and can meet the requirement of real-time feedback control of robotic grasping and manipulation.

B. Comparison of measurement precision

The comparison of precision was carried out using the developed prototypes. We built a test platform and fixed the tactile sensor on a micro-motion stage. By adjusting the stage, the soft elastomer can contact a test object [see Fig. 14(a)]. Eleven high-precision steel balls with increasing diameters from 10 mm to 20 mm were selected to press the same position under positive pressure, with the same pressing depth. Based on the acquired location information of marker points, the ball diameters were then calculated by spherical surface fitting to evaluate the measurement precision of the prototypes.

The maximum depth of the sphere pressed into the soft elastomer is recorded as $|\Delta Z|_{max}$. Because of the contact slip, only the marker points near the contact center can always maintain the adhesion relationship with the sphere, so we exclude the points with z-directional displacement less than $0.8 * |\Delta Z|_{max}$. Fig. 14(b) shows the fitting results and root mean square errors. The fitted diameters deviate less from the actual value for the prototype with CMP than for the prototype with DMP. Although the distortion of markers is slight in this

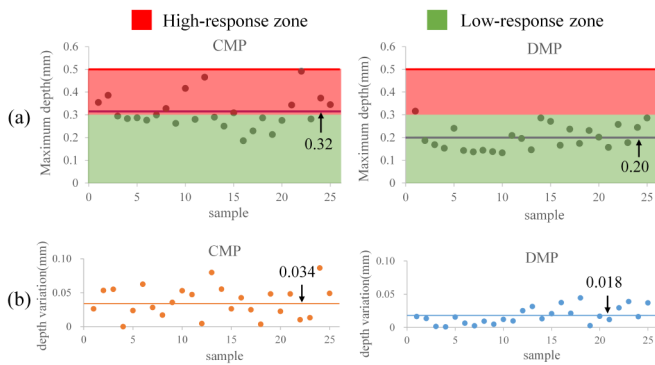


Fig. 15. Resolution comparison of tactile sensors. (a) Comparison of maximum depth values. (b) Comparison of gain values based on fitting.

experiment, the virtual marker points in CMP jointly participate in fitting the spherical diameter, which is equivalent to expanding the number of samples involved, thus making the fitting results more accurate.

Therefore, the CMP method can ensure high precision of measured marker points and further optimize the measurement by fitting and correcting virtual marker points, thus enhancing the precision of contact information representation.

C. Comparison of measurement resolution

The measurement resolution was compared based on the test platform built before, while the sphere was replaced with a tiny probe of 0.6 mm diameter. 25 sampling points were selected at equal intervals on the surface. We used the micro-motion stage to control the probe to press a depth of 0.5 mm at the corresponding sampling points. After each sampling, the marker point with the maximum z-directional displacement was selected to be the maximum depth value point. The closer the maximum depth is to the actual pressing depth, the better the responsiveness at that position, i.e., the higher the local resolution. Without loss of generality, we define 60% of the actual compression depth as the dividing line between high-response and low-response zones for qualitative analysis only. According to the simulation analysis in Section IV, the high-response zone should be the area that is close to the marker points.

Fig. 15(a) shows the distribution of the maximum depths. The maximum depth value at different sampling points captured is not the same, even for the same sensor. The results show that the average maximum depth value captured by the prototype with CMP is closer to the actual compression depth, and the number of sampling points falling in the high-response zone is significantly higher than that of the prototype with DMP. Further, the maximum depth values were corrected by polynomial fitting using the displacement values of the marker points around the maximum depth point [see Fig. 15(b)]. The average gain value of the sampling points in the tactile sensor with CMP is more significant, indicating that the fitted maximum depth values are closer to the actual depth.

Therefore, the CMP method can effectively expand the area of high-response zones and enhance the prototype's overall

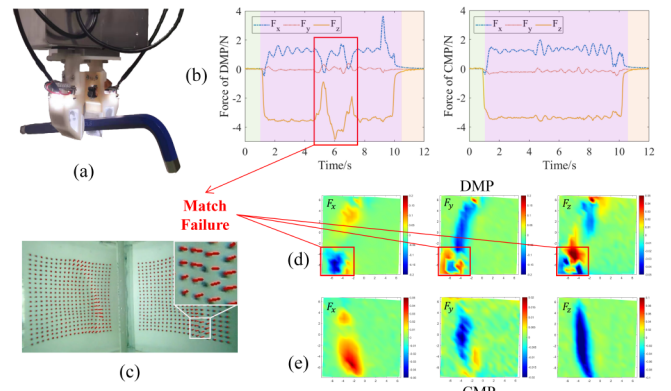


Fig. 16. Reliability comparison of tactile sensors (a) Experimental platform. (b) Comparison of contact distribution force measurements during grasping. (c) The matching tracking fails due to excessive displacement. (d), (e) The contact distribution forces measured by the two tactile sensors at that moment.

response capability, thus improving the resolution of contact information representation.

D. Comparison of measurement reliability

Finally, we carried out a grasping experiment to compare the measurement reliability. As shown in Fig. 16(a), the developed prototypes were mounted on a parallel gripper, which acted as the contact information measurement elements and as the end-effectors for grasping. A ROKAE XMate robotic arm was used to control the manipulator to grasp a hexagonal wrench in the grasping experiment, and artificial perturbations were applied during the gripping process to help with the evaluation of the measurement results under interference [see Fig. 16(a)].

By constructing a physical model of the soft elastomer, the contact distribution force can be reconstructed using the methods mentioned in our previous work [31]. Fig. 16(b) shows the contact forces measured by the two prototypes during the whole grasping process, including three stages: clamping the object, applying a disturbance, and releasing the object. When the hexagonal wrench is subjected to a significant disturbance, the prototype with DMP has a large deviation in the contact force measurement. In contrast, the tactile sensor with CMP has high measurement reliability and perfectly records the contact force information during the whole grasping process.

When a significant wobble occurs, the displacement of the marker points between adjacent frame images increases. For the prototype with DMP, when the amount of displacement is close to the distance between adjacent marker points in numerical value, the non-rigid matching method is easy to make errors [see Fig. 16(c)], so the corresponding contact distribution force solution does not match the actual situation at all [see Fig. 16(d), 16(e)]. If the measurement results are used to guide the gripping force regulation of the manipulator, it will undoubtedly lead to a failure of gripping. In contrast, the prototype with CMP can determine the order number of marker points according to the rigid matching method proposed to achieve high-reliability matching tracking and can still ensure the reliability of contact information representation even under severe contact working

TABLE I
COMPARISON OF OUR CMP AND EXISTING DMP

	CMP of Tac3D	DMP of GelForce [19]	DMP of GelSight [20]	DMP of Tactip [21]
Feature Type of Patterns	Continuous	Distributed	Distributed	Distributed
Information Density of Markers (cm^{-2})	189 + 2078 (virtual makers)	120×2 (2 layers)	83	178
Point-set Matching Method	Rigid	Non-rigid	Non-rigid	Non-rigid

conditions.

E. Comparison with DMP methods in other tactile sensors

To further illustrate the contribution of the proposed CMP method, we compare it with other vision-based tactile sensors that have adopted the DMP method. The metrics we focus on are only about the fineness and rigidity of the tactile information representation under ideal conditions, not the performance of the tactile sensors themselves.

The comparison details are stated in Table 1. The feature type is about the arrangement of feature information in the patterns, and the information density is expressed by the number of markers in the unit area. Table 1 shows that compared with the existing DMP methods, the core advantages of the CMP method are the continuity and richness of information representation and the rigidity of information extraction.

Although the performance of tactile sensors is related to a variety of factors, the representation of contact information determines the raw information of tactile perception and therefore has a greater impact on it. The above experimental results illustrate that sensors based on CMP have improved fineness and robustness in contact information measurement. Due to the universality of the proposed CMP principle, sensors with different configurations can also be improved by adopting the CMP method for information detection.

VI. CONCLUSION

This article proposes a new idea to deal with the shortcomings of traditional distributed marker patterns (DMP) in the information characterization of vision-based tactile sensor: continuous marker patterns (CMP), and gives a concrete implementation scheme. Three essential elements are abstracted: ideal gridlines, measured marker points, and virtual marker points. The proposed CMP method breaks through the inherent defects of the DMP method in principle. Compared with the DMP method, it can achieve higher precision, resolution, and reliability in representing contact information. Comparative experiments using the simulation analysis and the prototype experiments, respectively, verify the effectiveness and superiority of the CMP method.

The designs and basic principles of CMP are universal and inspiring in the high-quality information representation in

vision-based tactile sensors. This research will open up ideas for research in marker pattern methods and provide valuable references for innovating information representation methods. As future works, we will focus on expanding the designs and the corresponding information extraction algorithms, exploring the advantages of the CMP method in multimodal tactile information characterization, and optimizing the preparation process. The application of learning-based techniques for tactile information characterization and extraction is also the focus of our future research. We hope to promote the application of CMP in vision-based tactile sensors and provide better-performing tactile sensory components for robotics.

REFERENCES

- [1] M. J. Mataric, "Socially assistive robotics: Human augmentation versus automation," *Sci. Robot.*, vol. 2, no. 4, pp. eaam5410, Mar. 2017.
- [2] H. Huang, C. Yang, and C. L. P. Chen, "Optimal robot-environment interaction under broad fuzzy neural adaptive control," *IEEE Trans. Cybern.*, vol. 51, no. 7, pp. 3824–3835, Jul. 2021.
- [3] S. Ikemoto, H. B. Amor, T. Minato, B. Jung, and H. Ishiguro, "Physical human-robot interaction: Mutual learning and adaptation," *IEEE Robot. Autom. Mag.*, vol. 19, no. 4, pp. 24–35, Dec. 2012.
- [4] Y. Rizk, M. Awad, and E. W. Tunstel, "Cooperative heterogeneous multi-robot systems: A survey," *ACM Comput. Surv.*, vol. 52, no. 2, pp. 1–31, March. 2020.
- [5] R. Dahiya, G. Metta, M. Valle, and G. Sandini, "Tactile sensing: From humans to humanoid," *IEEE Trans. Robot.*, vol. 26, no. 1, pp. 1–20, Feb. 2010.
- [6] Y. Liu, R. Bao, J. Tao, J. Li, M. Dong, and C. Pan, "Recent progress in tactile sensors and their applications in intelligent systems," *Sci. Bull.*, vol. 65, no. 1, pp. 70–88, Jan. 2020.
- [7] Z. Kappassov, J.-A. Corrales, and V. Perdereau, "Tactile sensing in dexterous robot hands—Review," *Robot. Auton. Syst.*, vol. 74, pp. 195–220, Dec. 2015.
- [8] L. V. Duong and V. A. Ho, "Large-scale vision-based tactile sensing for robot links: Design, modeling, and evaluation," *IEEE Trans. Robot.*, vol. 37, no. 2, pp. 390–403, Apr. 2021.
- [9] Y. Zhang, J. Ye, Z. Lin, S. Huang, H. Wang, and H. Wu, "A piezoresistive tactile sensor for a large area employing neural network," *Sensors*, vol. 19, no. 1, pp. 27, 2019.
- [10] W. Lin, B. Wang, G. Peng, Y. Shan, H. Hu, and Z. Yang, "Skin-inspired piezoelectric tactile sensor array with crosstalk-free row plus column electrodes for spatiotemporally distinguishing diverse stimuli," *Adv. Sci.*, vol. 8, no. 3, pp. 2002817, Feb. 2021.
- [11] J. G. V. da Rocha, P. F. A. da Rocha, and S. Lanceros-Mendez, "Capacitive sensor for three-axis force measurements and its readout electronics," *IEEE Trans. Instrum. Meas.*, vol. 58, no. 8, pp. 2830–2836, Aug. 2009.
- [12] A. Mohammadi, Y. Xu, Y. Tan, P. Choong, and D. Oetomo, "Magnet-ic-based soft tactile sensors with deformable continuous force transfer medium for resolving contact locations in robotic grasping and manipulation," *Sensors*, vol. 19, no. 22, pp. 4925, 2019.
- [13] K. Shimonomura, "Tactile image sensors employing camera: A review," *Sensors*, vol. 19, no. 18, pp. 3933, 2019.
- [14] F. R. Hogan, M. Jenkin, S. Rezaei-Shoshtari, Y. Girdhar, D. Meger, and G. Dudek, "Seeing through your skin: Recognizing objects with a novel visuotactile sensor," in *Proc. IEEE Winter Conf. Appl. Comput. Vis.*, 2021, pp. 1218–1227.
- [15] Y. Wang, W. Ding, and D. Mei, "Development of flexible tactile sensor for the envelop of curved robotic hand finger in grasping force sensing," *Measurement*, vol. 180, pp. 109524, Aug. 2021.
- [16] R. Sui, L. Zhang, T. Li, and Y. Jiang, "Incipient slip detection method with vision-based tactile sensor based on distribution force and deformation," *IEEE Sensors J.*, vol. 18, no. 22, pp. 25973–25985, Oct. 2021.
- [17] T. Okatani and I. Shimoyama, "A tactile sensor for simultaneous measurements of 6-axis force/torque and the coefficient of static friction," *Sens. Actuators A, Phys.*, vol. 315, pp. 112362, Nov. 2020.

- [18] W. Yuan, C. Zhu, A. Owens, M. A. Srinivasan, and E. H. Adelson, "Shape-independent hardness estimation using deep learning and a gel-sight tactile sensor," in *Proc. IEEE Int. Conf. Robot. Autom.*, 2017, pp. 951-958.
- [19] K. Kamiyama, K. Vlack, T. Mizota, H. Kajimoto, N. Kawakami, and S. Tachi, "Vision-based sensor for real time measuring of surface traction," *IEEE Comput. Graph. Appl.*, vol. 25, no. 1, pp. 68-75, Jan./Feb. 2005.
- [20] W. Yuan, S. Dong, and E. H. Adelson, "Gelsight: High-resolution robot tactile sensors for estimating geometry and force," *Sensors*, vol. 17, no. 12, pp. 2762, 2017.
- [21] B. Winstone, G. Griffiths, C. Melhuish, T. Pipe, and J. Rossiter, "TACTIP - tactile fingertip device, challenges in reduction of size to ready for robot hand integration," in *Proc. IEEE Int. Conf. Robot. Biomimetics.*, 2012, pp. 160-166.
- [22] A. Yamaguchi and C. G. Atkeson, "Combining finger vision and optical tactile sensing: reducing and handling errors while cutting vegetables," in *Proc. IEEE-RAS 16th Int. Conf. Humanoid Robots.*, Nov. 2016, pp. 1045-1051.
- [23] M. Lambeta et al., "DIGIT: A novel design for a low-cost compact high-resolution tactile sensor with application to in-hand manipulation," *IEEE Robot. Autom. Lett.*, vol. 5, no. 3, pp. 3838-3845, Jul. 2020.
- [24] S. Choi and K. Tahara, "Development of a Visual-Tactile Fingertip Sensor and an Object Manipulation Method using a Multi-Fingered Robotic Hand", in *Proc. IEEE/SICE Int. Symp. Syst. Integr.*, 2020, pp. 1008-1015.
- [25] C. Sferrazza and R. D'Andrea, "Design, motivation and evaluation of a full-resolution optical tactile sensor," *Sensors*, vol. 19, no. vol. 4, pp. 928, 2019.
- [26] S. Wang, M. Lambeta, P.-W. Chou, and R. Calandra, "Tacto: A fast, flexible and open-source simulator for high-resolution vision-based tactile sensors," Dec. 2020. *arXiv preprint arXiv: 2012.08456*.
- [27] P. Ruppel, Y. Jonetzko, M. Gorner, N. Hendrich, and J. Zhang, "Simulation of the SynTouch BioTac Sensor," in *Proc. Int. Conf. Intell. Adv. Syst.*, 2018, pp. 374-387.
- [28] Z. Ding, N.F. Lepora, and E. Johns, "Sim-to-real transfer for optical tactile sensing," in *Proc. IEEE Int. Conf. Robot. Autom.*, 2020, pp. 1639-1645.
- [29] A. Agarwal, T. Man, and W. Yuan, "Simulation of vision-based tactile sensors using physics-based rendering," in *Proc. IEEE Int. Conf. Robot. Autom.*, 2021, pp. 1-7.
- [30] C. Sferrazza, T. Bi, and R. D'Andrea, "Learning the sense of touch in simulation: a sim-to-real strategy for vision-based tactile sensing," in *Proc. IEEE/RSJ Int. Conf. Intell. Robots Syst.*, 2020, pp. 4389-4396.
- [31] L. Zhang, Y. Wang, and Y. Jiang, "Tac3D: a novel vision-based tactile sensor for measuring force distribution and estimating friction coefficient distribution," Feb. 2022. *arXiv preprint arXiv: 2202.06211*.
- [32] S. N. Raza, H. R. U. Rehman, S. G. Lee and G. S. Choi, "Artificial Intelligence based Camera Calibration", in *Proc. Int. Wireless Commun. Mobile Comput. Conf.*, 2019, pp. 1564-1569.



Mingxuan Li was born in Huaihua City, Hunan Province, China in 2001. He is currently pursuing the B.E. degree in mechanical engineering from Tsinghua University, Beijing, China. His research interests include tactile sensing.



Lunwei Zhang was born in Hanzhong City, Shaanxi Province, China in 1995. He received the B.E. degree in mechanical engineering from Beihang University, Beijing, China, in 2021. He is currently working towards the Ph.D. degree at Tsinghua University, Beijing, China. His research interests include tactile sensing and force reconstruction.



Tiemin Li received the B.S. degree from the Qiqihar Institute of Light Industry, Heilongjiang, China, in 1991, the master's degree from the Harbin Institute of Technology, Heilongjiang, China, in 1996, and the Ph.D. degree from Tsinghua University, Beijing, China, in 2000, all in mechanical engineering.

He is currently an Associate Professor with the Department of Mechanical Engineering, Tsinghua University. His current research interests include advanced manufacturing technology, robotics, and parallel kinematic machines.



Yao Jiang (M'16) received the B.S. degree from the Nanjing University of Science and Technology, Nanjing, China, in 2011, and the Ph.D. degree from Tsinghua University, Beijing, China, in 2016, both in mechanical engineering.

From 2016 to 2017, he was a Postdoctoral Researcher with the Department of Precision Instrument, Tsinghua University. From 2017 to 2018, he was a Postdoctoral Researcher with Harvard School of Engineering and Applied Sciences. He is currently an Assistant Professor with the Department of Mechanical Engineering, Tsinghua University. His current research interests include tactile sensing, robotic grasping and manipulation, computer vision metrics, and mobile robot.